Simulating Mechanism of Brain Injury During Closed Head Impact

Omar Halabieh[1] and Justin W.L. Wan[2]

[1] David R. Cheriton School of Computer Science, University of Waterloo, Waterloo, ON N2L 3G1, Canada
ohalabie@uwaterloo.ca
[2] David R. Cheriton School of Computer Science, University of Waterloo, Waterloo, ON N2L 3G1, Canada
jwlwan@uwaterloo.ca

Abstract. In this paper, we study the mechanics of the brain during closed head impact via numerical simulation. We propose a mathematical model of the human head, which consists of three layers: the rigid skull, the cerebrospinal fluid and the solid brain. The fluid behavior is governed by the Navier-Stokes equations, and the fluid and solid interact together according to the laws of mechanics. Numerical simulations are then performed on this model to simulate accident scenarios. Several theories have been proposed to explain whether the ensuing brain injury is dominantly located at the site of impact (coup injury) or at the site opposite to it (contrecoup injury). In particular, we investigate the positive pressure theory, the negative pressure theory, and the cerebrospinal fluid theory. The results of our numerical simulations together with pathological findings show that no one theory can explain the mechanics of the brain during the different types of accidents. We therefore highlight the accident scenarios under which each theory presents a consistent explanation of brain mechanics.

1 Introduction

Head injury sustained in accidents, for instance car crashes, continues to be a leading cause of death and disability. In US, millions of head injuries occurred every year. The associated socio-economic cost was estimated to be 60 billion dollars in 2000. Automobile accidents account for a large portion of these injuries, despite the use of modern protective measures such as seatbelts and airbags. For instance, data compiled by the National Center for Injury Prevention and Control in US shows that 20% of head injuries were due to motor vehicle traffic crashes. To be able to prevent head injuries and improve car safety design as well as patient diagnose and treatment, a better understanding of the mechanics of the head subjected to an impact is very important.

One particular type of brain injury of great interest is the coup-contrecoup contusion; it is frequently observed that the injury to the brain opposite to the location at which the head strikes an external object (contrecoup injury) is more severe than the injury to the brain that occurs adjacent to the impact site (coup

F. Bello, E. Edwards (Eds.): ISBMS 2008, LNCS 5104, pp. 107–118, 2008.

injury). This is known as the coup-contrecoup phenomenon. This observation has been extensively documented in pathological findings, following autopsies performed on victims [1,2,3,4,5]. Many theories have been developed to explain this counterintuitive phenomenon.

Three of the theories are: positive pressure, negative pressure and cerebrospinal fluid (CSF) theories. According to the positive pressure theory, presented by Lindenberg [1,6], as the head moves forward prior to impact, the brain tends to lag behind. Thus at the moment prior to impact, the lagging part of the brain is compressed against the skull at the contrecoup location while all the protective fluid is cushioning the coup site. At impact, a positive pressure wave amplifies the pre-existing compression of the brain tissue against the skull at the contrecoup location, causing the contrecoup injury. The negative pressure theory, presented by Russell [5,7,8], explains that once the skull is suddenly stopped at impact, the brain continues to move forward due to inertia. This results in an increase in the tensile force developing at the contrecoup site (negative pressure). This tensile force eventually leads to tearing of tissue and bridging vessels at the contrecoup location. The CSF theory was suggested by Drew [9]. It assumes that CSF is denser than brain tissue. Thus, the brain at impact is propelled to the contrecoup location due to the CSF moving forward towards the coup site.

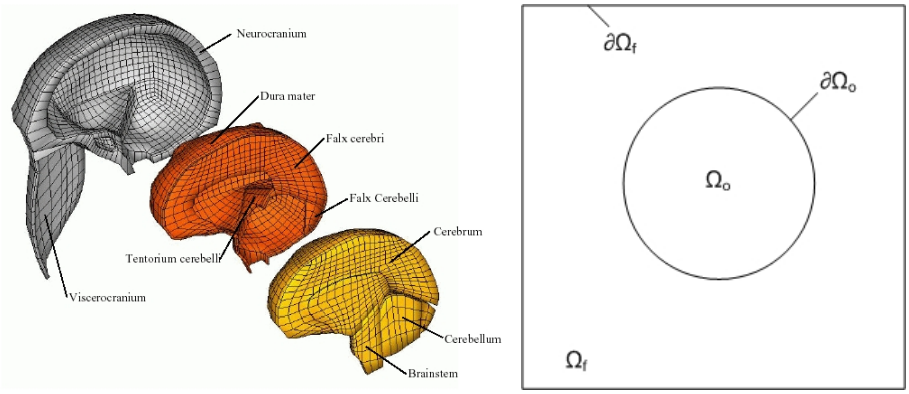

Fig. 1. (Left) A finite element model of the human head [11], (right) the proposed head model has 3 layers: skull ($\partial\Omega_f$), CSF (Ω_f), and the brain (Ω_o)

Numerical models have been developed to understand the mechanisms of this injury through simulations [11,12,13,14]. However these models have either ignored the role of the CSF or modeled it incorrectly as solid. In this paper, we propose a new head modeling approach based on the correct representation of the CSF as a fluid. More precisely, the head model is made up of three layers: the rigid skull, the CSF and finally the solid brain. Since the CSF plays such a crucial role as "a neuro-protective layer that absorbs shear energy" [7], a correct modeling of CSF is necessary to better understand the brain injury mechanism. We note that while the deformations of the skull and the brain are also important

aspects of head injury, the primary focus of this paper is on how CSF affects the the motion of the brain that leads to the coup-contrecoup phenomenon. We refer the interested readers to [15,16] for mechanical response of the skull modeled as deformable shells during direct impact.

In Section 2, we present our mathematical model of the head and discuss the governing equations for the motion of each component and their interaction. Then, in Section 3, we discuss the numerical solution of the model equations. In particular, we present techniques to accurately locate the fluid-solid interface as well as numerical methods to deal with quantities near the interface. In Section 4, results of the simulations are then presented, discussed and tied in with existing theories. Finally, concluding remarks are made in Section 5.

2 Mathematical Model

There are several existing 2D/3D mathematical head models, e.g. [11,12,13,14]. Generally speaking, these models are usually based on exact geometry of the human head, see Fig. 1 (left). The modeled anatomical structures vary but usually include the skull, meningeal layers, and the brain. The skull is modeled as rigid [11] or linear elastic solid [12,13,14], the meningeal layers as linear elastic solid [11,12], and the brain as quasi-linear [12] or nonlinear viscoelastic solid [14]. There are also brain models based on viscoelastic fluid [17,18]. Then, simulations are often performed using commercial finite element softwares such as MADYMO [11] and ANSYS [13,14]. While these softwares allow the user to reliably solve complex problems, they are typically either specialized in solid or fluid calculations, rarely both at the same time. It partially explains why CSF is often omitted or modeled as a solid [11,14]. Here, we propose a mix fluid-solid head model which is more faithful to the constituent mechanical properties.

As discussed in Section 1, our primary interest is to study the coup-contrecoup phenomenon. Thus, our 2D head model as shown in Fig. 1 (right) is not intended to be elaborate nor contain accurate anatomical features. Rather, it will focus on the role of CSF plays in the coup-contrecoup phenomenon. The outer square represents the skull and the inner circle represents the brain. In between the two is the space of CSF. The particular shapes are not based on anatomical reasons but for the convenience of the numerical computation. Note that since the essence of the coup-contrecoup study is how CSF affects the motion of the brain relative to the head, we find that the particular shapes do not play a crucial role here. The following describes the model equations for each component.

Cerebrospinal fluid. CSF is modeled via the incompressible Navier-Stokes equations. These equations enforce the conservation of mass and conservation of momentum laws. Let $\mathbf{u}(x,t)$ be the velocity vector at position $\mathbf{x}$ and time t and p be the pressure. Then the motion of the fluid is governed by the equations:

$$\begin{aligned} \frac{\partial}{\partial t}\mathbf{u} + (\mathbf{u}\cdot\nabla)\mathbf{u} + \nabla p = \frac{1}{Re}\triangle\mathbf{u} + \mathbf{g} \qquad & \mathbf{x}\in\Omega_f, \\ \nabla\cdot\mathbf{u} = 0 \qquad & \mathbf{x}\in\Omega_f, \end{aligned} \tag{1}$$

where $\mathbf{g}$ is the gravity and Re is the so-called Reynolds number.

Fluid/solid interaction. An object immersed in a fluid is subject to a total force, $\mathbf{F}$, given by the following equations:

$$\mathbf{F} = \int_S \boldsymbol{\tau} \cdot \mathbf{n} \, dA + \mathbf{G}, \tag{2}$$

where $\boldsymbol{\tau}$ is the hydrodynamic stress tensor, and $\mathbf{n}$ the outward-pointing normal vector on the surface S. The stress tensor $\boldsymbol{\tau}$ is given by [19]:

$$\boldsymbol{\tau} = -p\mathbf{I} + \mu(\nabla\mathbf{u} + \nabla\mathbf{u}^T), \tag{3}$$

where μ is the fluid viscosity. The first term in the equation refers to the force contribution due to the hydrostatic pressure, while the second term refers to the force contribution due to the viscosity/friction in the fluid. The net gravitational force, $\mathbf{G}$, acting on the object is given by: $\mathbf{G} = V_o(\rho_o - \rho_f)\mathbf{g}$, where V_o is the volume of the object, ρ_o the object density and ρ_f the fluid density.

Interface modeling. As the object moves in the fluid, we model the interface motion using the level set method [20], which has achieved notable success in a wide area of applications [21,22]. The interface is represented implicitly by the zero level set of a function ϕ. For example, to represent a circle of radius r in 2D, the level set function can be defined as a cone: $\phi(x, y) = \sqrt{x^2 + y^2 - r^2}$. For more general curves, numerical techniques are needed [21,22]. The region where $\phi < 0$ denotes the object and the region where $\phi > 0$ denotes the fluid. It helps us distinguish our computational domain into a fluid domain and an object domain. As the object moves, the values of the level set function ϕ are updated by solving the following equation:

$$\phi_t + \mathbf{u} \cdot \nabla\phi = 0. \tag{4}$$

Equations (1)-(4) form the governing equations for our 2D head model.

3 Numerical Solution

The numerical solution procedure involves several steps in each time stepping.

Step 1: computational domain. The Navier-Stokes equations are solved on a finite difference staggered grid consisting of grid cells. Since the equations are only defined in the fluid domain, a major issue is that we need to be able to identify fluid cells and the object cells using the values of $\{\phi_{i,j}\}$ at the grid points. We use a method similar to the one described in [23]. The idea is to determine the portion of the cell occupied by fluid and the portion occupied by the object. The dominant portion will then dictate the nature of the cell. We first give all cells the label C_F (fluid cells). Now, we identify nine different scenarios under which the cell label will be modified to C_B (object cells); see Fig. 2. The signs (+ and -) denote the sign of $\phi_{i,j}$ at the 4 corners. The top four cases mark the cell as C_B since the object occupies the major portion of the cell.

In the bottom four cases, we first determine the coordinates of the points (xa, xa2, etc) at which the interface intercepts the grid cell. This is done via linear interpolation of the two level set function values with opposite signs. Then we check to see if consequently the majority of the cell is occupied by the object. If so, the cell is labeled C_B. The last case (not shown in Fig. 2) is when four level set values are negative, thus indicating an object cell.

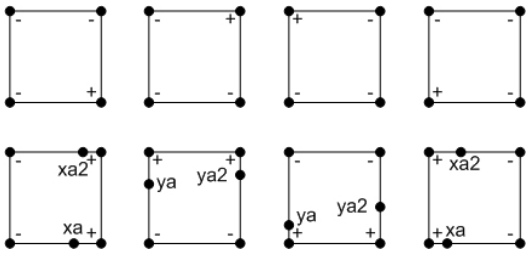

Fig. 2. The eight configurations for which a cell is labeled as an object cell

The boundary object cells are then identified, which can be classified into 8 types: B_N, B_W, B_E, B_S, B_NE, B_SE, B_NW, and B_SW. This labeling is based on which neighbors of an object cell are fluid. For example, B_SE denotes an object cell who's fluid neighbors are its southern and eastern neighbors. The other boundary object cell types are defined analogously.

Step 2: solve Navier-Stokes and boundary conditions. After the cell identification step, the Navier-Stokes equations are solved on the fluid domain using finite difference method. In solving the equations numerically, we also need to enforce that the fluid and object should have the same velocity at the interface. Consider a B_N cell (i, j) with a configuration illustrated in the Fig. 3. We assign values for $u_{i-1,j}$, $u_{i,j}$, and $v_{i,j}$ to satisfy the boundary condition. We first compute the coordinates of the points $y1$ and $y2$ at which the interface cuts the grid cell by linear interpolation. Then we derive the formulas for the boundary values as follows:

$$
\begin{aligned}
v_{i,j} &= \left(\frac{h-(y1+y2)/2}{2h-(y1+y2)/2}\right) v_{i,j+1} + \left(\frac{h-2h}{(y1+y2)/2-2h}\right) v_{object}, \\
u_{i-1,j} &= \left(\frac{h/2-y2}{3h/2-y2}\right) u_{i-1,j+1} + \left(\frac{h/2-3h/2}{y2-3h/2}\right) u_{object}, \\
u_{i,j} &= \left(\frac{h/2-y1}{3h/2-y1}\right) u_{i,j+1} + \left(\frac{h/2-3h/2}{y1-3h/2}\right) u_{object},
\end{aligned}
$$

where (u_{object}, v_{object}) is the velocity of the object. Other cell types and level set configurations are treated similarly (omitted here).

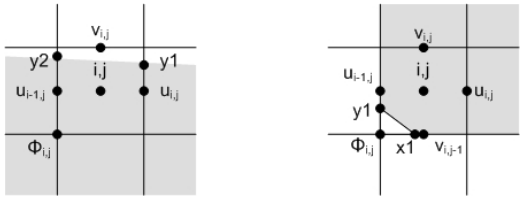

Fig. 3. B_N (left) and B_SW (right) type boundary object cells (grey: object, white: fluid)

Step 3: surface force. The force exerted by the fluid on the solid needs to be calculated. First, the equations for the stress tensor (3) are discretized on each boundary object cell. Note that the discretization depends on the type of the boundary object cell (i.e. B_N, B_W, etc). Once $\boldsymbol{\tau}$ is computed, then the force exerted on this cell is: $\boldsymbol{F_{i,j}} = \boldsymbol{\tau}\triangle x$. The total force on the object is then computed by summing over all boundary object cells. We remark that we ignore the net gravitational force term $\boldsymbol{G}$ in (2) since physiologically the brain is tethered through the brain stem and spinal cord. Once the force $\mathbf{F}$ is computed, the acceleration of the object is calculated via Newton's second law: $\mathbf{a} = \boldsymbol{F}/m$, where m is the mass of the object. From the acceleration, the velocity of the object at time step $n+1$ can be updated.

Step 4: interface motion. Finally, the object velocity computed from previous step is used to evolve the level set function according to (4) which is also solved using finite difference method.

4 Simulation and Results

The main focus of our simulations is to analyze the motion of the brain and how it depends on brain density, brain size, and head velocity. Head impact accident can be thought of as happening in two phases. The first phase is the initial acceleration of the head prior to impact (it might not be present in all accidents). The second phase is that of the actual impact. This happens when the head meets an object and comes to a full stop. The grid size for all the computations is 40×40. Other grid sizes have also been tested and they show similar qualitative results.

Phase 1: accelerating head prior to impact. The head is accelerating horizontally. There are two ways to incorporate this scenario in the numerical simulation. One is to set the fluid velocity $\mathbf{u}$ = velocity of the accelerating head on $\partial\Omega_f$. Another is to specify $\mathbf{u} = 0$ on $\partial\Omega_f$; thus, all the computed quantities are relative to the head (not the outside viewer). In this case, the initial condition for $\mathbf{u}$ inside Ω_f would be negative of the moving head velocity. The former may seem natural, but the latter is what we used since it better illustrates the relative motion of the brain to the head.

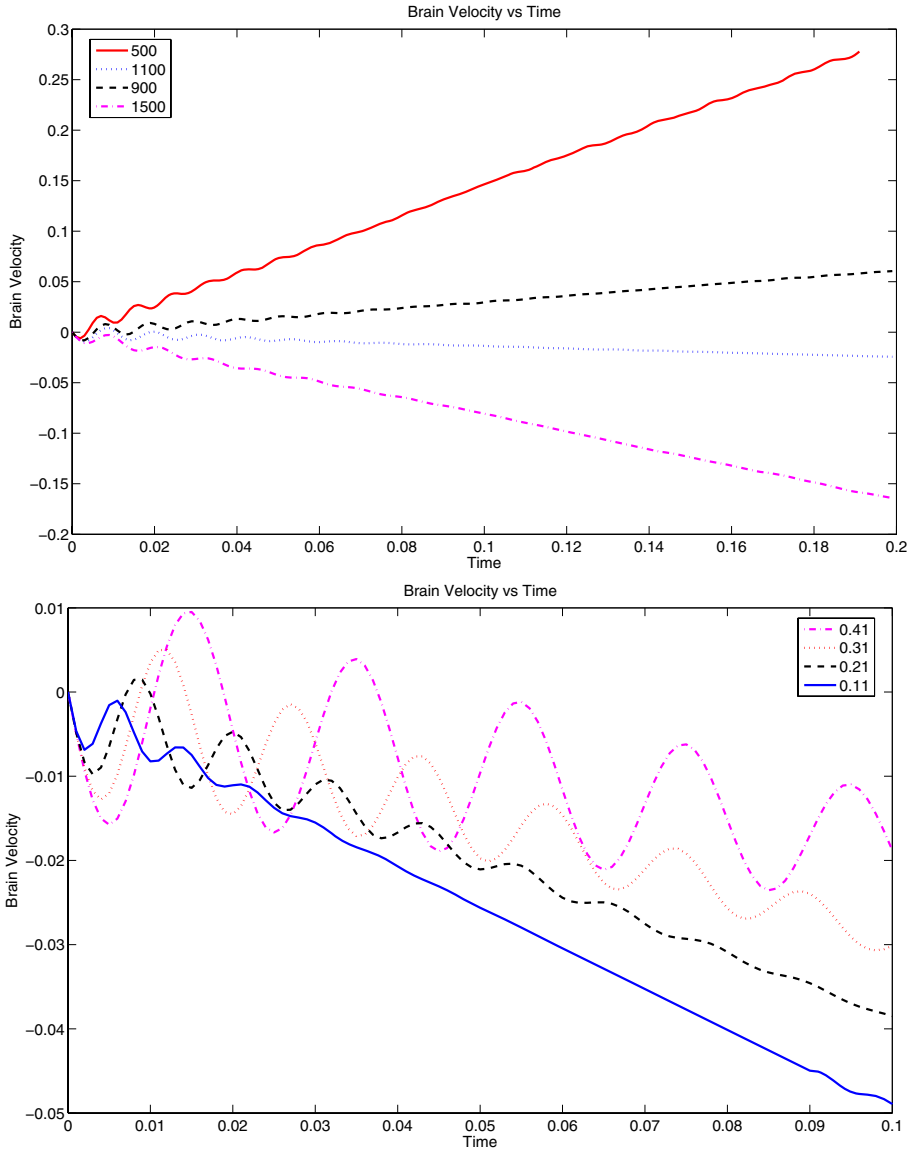

Fig. 4. Brain velocity relative to the moving head with (top) different brain density, and (bottom) different brain size

We perform the simulation to study the effect of brain density on its motion. The CSF density is fixed at $1000kg/m^3$ (the same as water), and the brain density varies from $500kg/m^3$ to $1500kg/m^3$. We remark that the actual brain density range is believed to be much smaller. This artificially wider testing range is used for the purpose of illustrating the qualitative behavior such that the

differences are more visible. Fig. 4 (top) shows the simulation results. If brain tissue is denser than CSF, as the head accelerates forward, the brain lags behind. On the other hand, if CSF is denser, then the brain also moves forward. Larger density difference results in larger velocity of the brain; however, the direction of motion is unchanged.

In the second simulation, we vary the brain radius from $r = 0.11$ to 0.41. Again, the range is for qualitative illustration only and they are by no means the actual sizes of human brains. Fig. 4 (bottom) shows that larger the brain size (thus heavier the brain), slower the velocity it attains. The direction, however, is unaffected by the size. We use $1200kg/m^3$ for the brain density in all cases and the brain always lags behind.

In the third simulation, we vary the acceleration of the moving head from $\mathbf{a} = 5m/s^2$ to $\mathbf{a} = 50m/s^2$. The brain velocity will be around 10 times larger at the final time. The direction of the brain is also unaffected. Thus, from the last two simulations, we can perform qualitative studies on brain motion with arbitrary head velocity and brain size.

Two aspects that are of importance: the brain movement and the CSF velocity field. Fig. 5 (top) shows snapshots of the brain position inside the head. The density of the brain is chosen to be less than CSF; we see that brain moving forward relative to the head, as the denser CSF lags behind. The velocity field of CSF is shown in Fig. 5 (bottom).

Phase 2: head at impact. To simulate this scenario, we set the boundary condition 0 on $\partial\Omega_f$. But since the head was moving at certain velocity $\mathbf{u}_{initial}$, so were the CSF and the brain. Thus the initial conditions for the velocities of the CSF and the brain are set to $\mathbf{u} = \mathbf{u}_{initial}$.

As in the previous phase, we study the effect of the brain density on its motion. As shown in Fig. 6 (top), if the brain is denser, as the head comes to a stop, the brain continues to more forward inside the head. On the other hand, if CSF is denser, then the brain moves backward. We also perform simulations with varying brain sizes and head speeds. The conclusions are similar to those in Phase 1; see Fig. 6 (bottom).

Verification of existing theories for closed head impact. As mentioned in Section 1, there are three main theories that have been developed to explain the coup-contrecoup phenomenon. The positive pressure and negative pressure theories implicitly assume that the CSF is less dense than brain tissue whereas the CSF theory assumes that CSF is denser than brain tissue by about 4%. In the human physiology literature, it is widely agreed upon that these two substances have very close densities; however, it is not clear which one is slightly denser than the other [24]. We will examine these theories based on the findings of our simulation results.

There are two accident scenarios that are of interest. The first scenario is when the head is accelerated by the impact; e.g. a head is being hit by a baseball bat. The second scenario is where the head is already in a state of acceleration at the moment of impact; e.g. the head of the driver hitting the steering wheel, or a

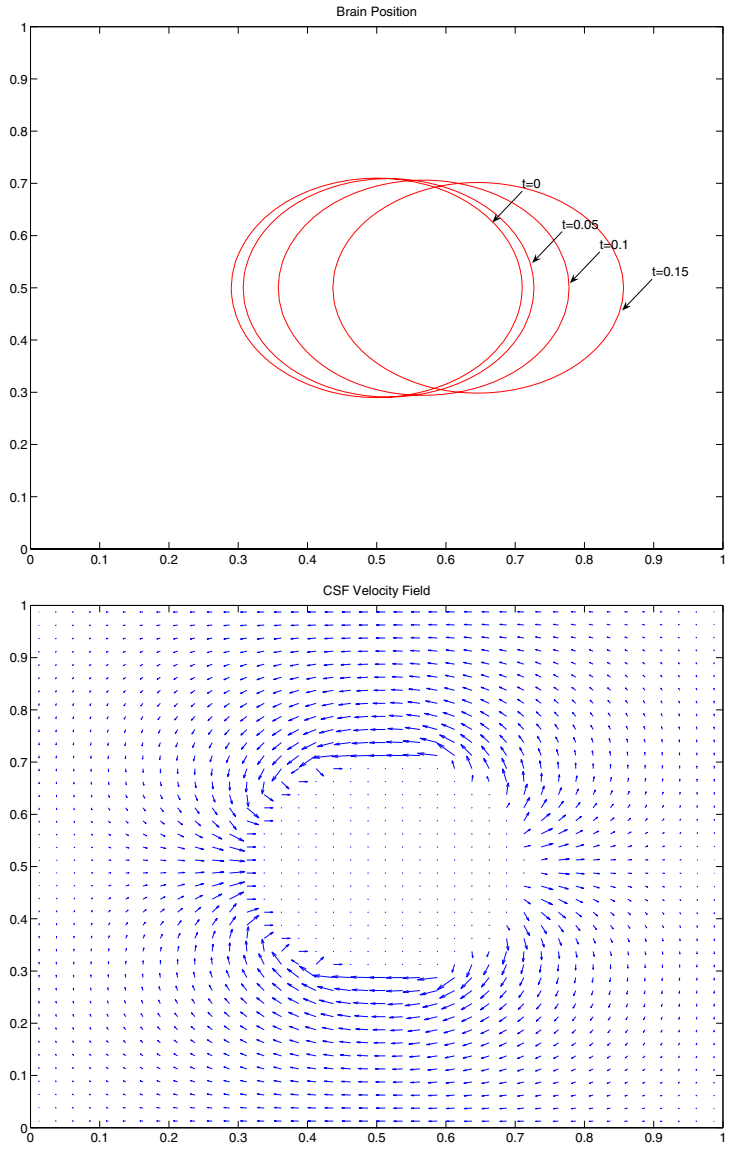

Fig. 5. (Top) Brain position at different times, (bottom) the velocity field of CSF as the brain moves to the right

fall/slip. Due to limited space, we will only discuss the second scenario. In such accidents, contrecoup injuries are usually dominant and coup injuries are minor or absent [1].

According to the positive pressure theory, as the head is accelerated prior to impact, the brain will lag behind and the less dense CSF will move to the

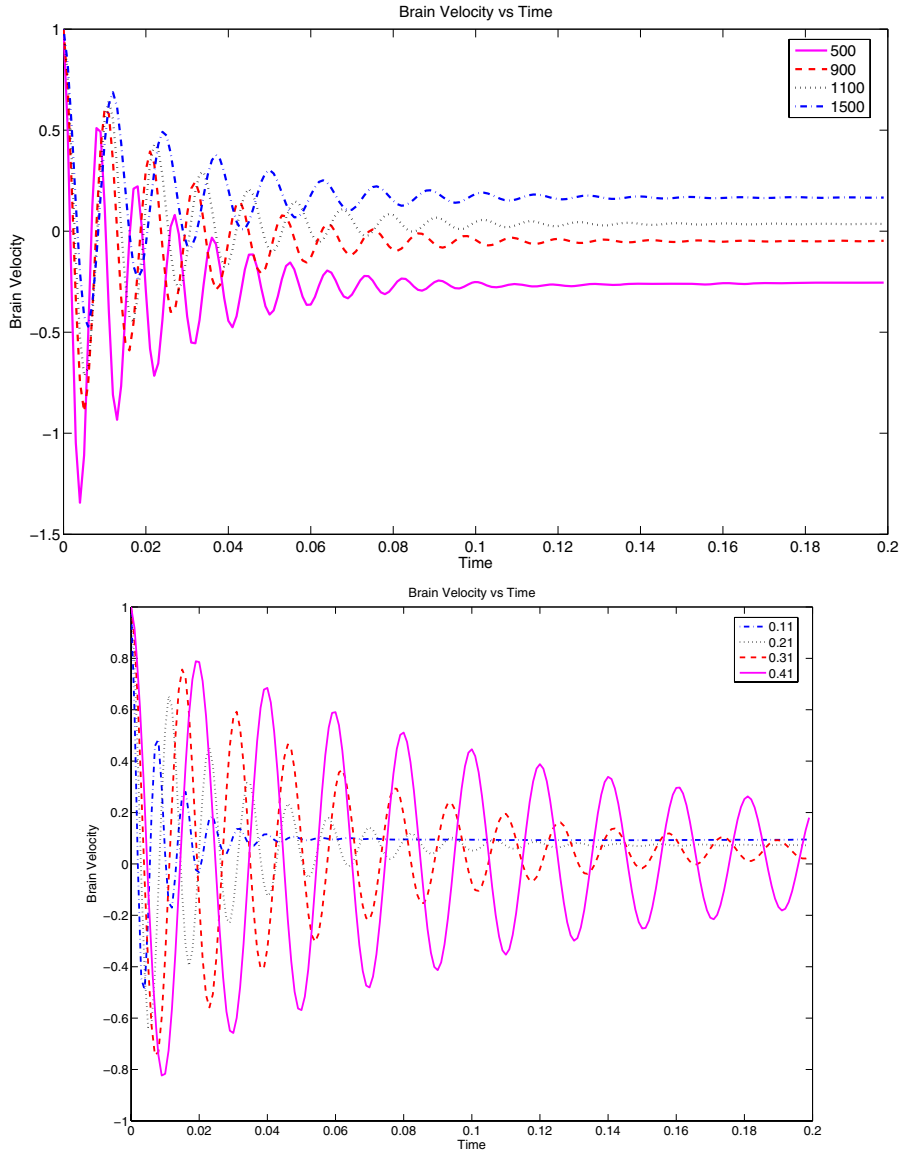

Fig. 6. Brain velocity relative to the moving head with (top) different brain density, and (bottom) different brain size

impact site. This is in fact what we observed in our simulations; see Fig. 4. Although qualitatively correct, there are drawbacks quantitatively. E.g. in a fall scenario, the acceleration that would lead to the positive pressure (lag) is about 1g, but it has been reported that the brain can withstand 40-80g's of relatively sustained acceleration without any brain injury. Thus to produce injury, the

head acceleration must come from impact compression. We conclude that the initial lag in this case cannot be the main cause for the severe contrecoup injury and that the positive pressure theory is not able to explain this observation.

According to the negative pressure theory, at impact, the brain will continue to move towards the impact site. This is what we observed in our simulation if the brain tissue is denser than CSF; see Fig. 6. However, the theory does not take into account the fact that as the head is accelerating, the brain will actually have shifted towards a lagging position just prior to impact. It may counteract the forward motion right after the impact. This configuration shift prior to impact is not taken into account in the negative pressure theory.

According to the CSF theory, at impact, the brain will move towards the contrecoup site. This is what we observed in our simulation if CSF is denser than the brain; see Fig. 6. The CSF theory, however, also does not take the initial phase of head acceleration into account. In this case, the less dense brain will actually have shifted towards the impact site just prior to impact. This again might counteract the backward motion later.

5 Conclusion

We have proposed a mathematical model of the human head, which consists of the rigid skull, the CSF and the solid brain. The CSF is modeled by the Navier-Stokes equations. A numerical solution procedure is presented to describe accurate techniques to capture the fluid and solid interaction through the interface. Simulations are performed to analyze the mechanism during a head impact. The simulation results are used to verify existing theories that explain the contrecoup injury. It turns out that no one theory is able to explain all observed pathological findings in different accident scenarios. More careful studies are needed for each type of accident scenarios. These studies should further probe the pathology of head injury to identify the nature of forces causing brain injury, whether tensile or compressive or both, given the clinical observations. In addition, further investigation is required in the physiology of the human head to discern the issue of whether CSF is more or less dense than brain tissue.

References

1. Lindenberg, R., Freytag, E.: The mechanism of cerebral contusions. AMA Archives of Pathology 69, 440–469 (1960)
2. Denny-Brown, D., Russell, W.R.: Experimental cerebral concussion. Brain 64, 95–164 (1941)
3. Denny-Brown, D.: Cerebral concussion. Neurological Unit, Boston City Hospital, and the Department of Neurology, Harvard Medical School
4. Gurdjian, E., Gurdjian, E.S.: Cerebral contusions: Re-evaluation of the mechanism of their development. The Journal of Trauma 16, 35–51 (1976)
5. Russell, W.: Cerebral involvement in head injury. Brain 55, 549 (1932)
6. Lindenberg, R.: Trauma of meninges and brain. In: Minckler, J. (ed.) Pathology of the nervous system. McGraw-Hill, New York (1971)

7. Dawson, S.L., Hirsh, C.S.: The contrecoup phenomenon, reappraisal of a classical problem. Human Pathology 11, 155–166 (1980)
8. Gross, A.: A new theory on the dynamics of brain concussion and brain injury. Journal of Neurosurgery 15, 548 (1958)
9. Drew, L.B., Drew, W.E.: The contrecoup-coup phenomenon-a new understanding of the mechanism of closed head injury. Neurocritical Care 4(3), 385–390 (2004)
10. for Neuro Skills, C, http://www.neuroskills.com/edu/ceuoverview5.shtml
11. Brands, D.: Predicting brain mechanics during closed head impact. PhD thesis, Eidhoven University of Technology (2002)
12. Belingardi, G., Chiandussi, G., Gaviglio, I.: Development and validation of a new finite element model of human head. Technical report, Politecnio di Torino, Dipartimento di Meccanica, Italy (2005)
13. Chu, C.S., Lin, M.S., Huang, H.M., Lee, M.C.: Finite element analysis of cerebral contusion. Journal of Biomechanics 27(2), 187–194 (1994)
14. Chu, Y., Bottlang, M.: Finite element analysis of traumatic brain injury. In: Legacy Clinical Research and Technology Center, Portland, OR,
15. Engin, A.E.: The axisymmetric response of a fluid-filled spherical shell to a local radial impulse–a model for head injury. Journal of Biomechanics 2, 325–341 (1969)
16. Kenner, V., Goldsmith, W.: Impact on a simple physical model of the head. Journal of Biomechanics 6, 1–11 (1973)
17. Cotter, C.S., Szczyrba, P.S.I.: A viscoelastic fluid model for brain injuries. International Journal for numerical methods in fluids 40, 303–311 (2002)
18. Szczyrba, I., Burtscher, M.: On the role of ventricles in diffuse axonal injuries. In: Summer Bioengineering Conference (2003)
19. Landau, L., Lifshitz, E.: Fluid Mechanics. Pergamon Press, Oxford (1987)
20. Osher, S., Sethian, J.A.: Fronts propagating with curvature-dependent speed:algorithms based on hamilton-jacobi formulation. Journal of Computational Physics 79, 12–49 (1988)
21. Sethian, J.A.: Level Set Methods and Fast Marching Methods, 2nd edn. Cambridge University Press, Cambridge (1999)
22. Osher, S., Fedkiw, R.: Level Set Methods and Dynamic Implicit Surfaces. Springer, Heidelberg (2003)
23. Tome, M.F., McKee, S.: Gensmac: A computational marker and cell method for free surface flows in general domains. Journal of Computational Physics 110, 171–186 (1994)
24. Guyton, A., Hall, J.: Textbook of Medical Physiology, 11th edn. Elsevier Sauders, Amsterdam (2006)